How to cite: *Angew. Chem. Int. Ed.* **2025**, *64*, e202417889
doi.org/10.1002/anie.202417889

Hydrogen Isotope Exchange | Hot Paper

Hexafluorophosphate-Triggered Hydrogen Isotope Exchange (HIE) in Fluorinated Environments: A Platform for the Deuteration of Aromatic Compounds via Strong Bond Activation

*Yang Ni, Jonathan Lebelt, Milena Barp, Florian Kreuter, Hannah Buttkus, Jiaye Jin, Martin Kretzschmar, Ralf Tonner-Zech, Knut R. Asmis, and Tanja Gulder**

Abstract: There is a perpetual need for efficient and mild methods to integrate deuterium atoms into carbon frameworks through late-stage modifications. We have developed a simple and highly effective synthetic route for hydrogen isotope exchange (HIE) in aromatic compounds under ambient conditions. This method utilizes catalytic amounts of hexafluorophosphate (PF_6^-) in deuterated 1,1,1,3,3,3-hexafluoroisopropanol (HFIP-d_1) and D_2O. Phenols, anilines, anisoles, and heterocyclic compounds were converted with high yields and excellent deuterium incorporations, which allows for the synthesis of a wide range of deuterated aromatic compounds. Spectroscopic and theoretical studies show that an interactive H-bonding network triggered by HFIP-d_1 activates the typically inert P–F bond in PF_6^- for D_2O addition. The thus in situ formed DPO_2F_2 then triggers HIE, offering a new way to deuterated building blocks, drugs, and natural-product derivatives with high deuterium incorporation via the activation of strong bonds.

[*] Dr. Y. Ni, Prof. Dr. T. Gulder
Biomimetic Catalysis, Catalysis Research Center, TUM School of Natural Sciences, Technical University of Munich, Lichtenbergstrasse 4, 85748 Garching, Germany

Dr. Y. Ni, J. Lebelt, Dr. M. Kretzschmar, Prof. Dr. T. Gulder
Institute of Organic Chemistry, Faculty of Chemistry and Mineralogy, Leipzig University, Johannisallee 29, 04103 Leipzig, Germany

M. Barp, F. Kreuter, H. Buttkus, J. Jin, Prof. Dr. R. Tonner-Zech, Prof. Dr. K. R. Asmis
Wilhelm-Ostwald-Institut für Physikalische und Theoretische Chemie, Universität Leipzig, Linnéstraße 2, 04103 Leipzig, Germany

J. Lebelt, Prof. Dr. T. Gulder
Organic Chemistry—Biomimetic Catalysis, Saarland University, 66123 Saarbruecken, Germany
E-mail: tanja.gulder@uni-saarland.de

Prof. Dr. T. Gulder
Synthesis of Natural-Product Derived Drugs, Helmholtz Institute for Pharmaceutical Research Saarland (HIPS), Helmholtz Centre for Infection Research (HZI), 66123 Saarbruecken, Germany

Introduction

The pursuit of methods enabling facial integration of deuterium atoms into carbon skeletons via late-stage modifications has lately witnessed a dramatic increase in attention.[1] This pursuit extends across physical organic chemistry, target-oriented synthesis, medicinal chemistry, and chemical biology.[1b,2] Deuterium isotope labeling is a valuable tool for investigating the mechanisms of organic reactions in chemical and biological contexts or as internal standards in bioanalytic investigations using mass spectrometry.[3] In pharmaceutical development, substantial research efforts have been directed toward comprehending active pharmaceutical ingredients (APIs) in vivo pharmacokinetic and pharmacodynamic properties.[2a–c,4] Harnessing the kinetic isotope effect (KIE),[5] deuterium incorporation improves the drugs' absorption, distribution, metabolism, excretion, and toxicity (ADMET) profile in multiple ways. For example, it increases its lipophilicity, thereby enhancing its membrane penetration. It can also inhibit oxidative degradation, a pivotal pathway in drug metabolism.[6] Drug-target interactions can be strengthened in deuterated APIs compared to their H-analogs, leading to enhanced activities. Although deuterium incorporation in drug scaffolds was first published in the early 1960s,[7] it took until 2017 for the first deuterated drug, Deutetrabenazine (Austedo®), to be approved by the FDA for treating Huntington's-disease-related disorders.[8] This example opened the way for deuterium-containing medicines (Figure 1a), showcased by further deuterated drugs already introduced or on their way to the market.[9]

Considering these developments, there is an increasing potential and interest in obtaining deuterated products and building blocks efficiently, inexpensively, and simply suitable for large-scale manufacturing. Typically, deuterium-labeled compounds are synthesized using multi-step processes, often involving pre-functionalized starting materials, such as halogen- and pseudohalogen-containing compounds or phosphonium salts.[10] However, these conventional methods often involve time-consuming and expensive procedures, leading to poor atom economy. A promising alternative involves direct **h**ydrogen **i**sotope **e**xchange (HIE) through late-stage functionalization of the target molecule (Figure 1b).[1b,2d,4,11] HIE in aromatic compounds is particularly challenging as it necessitates the activation of strong C_{sp2}–H bonds, usually accomplished using strong Brønsted/

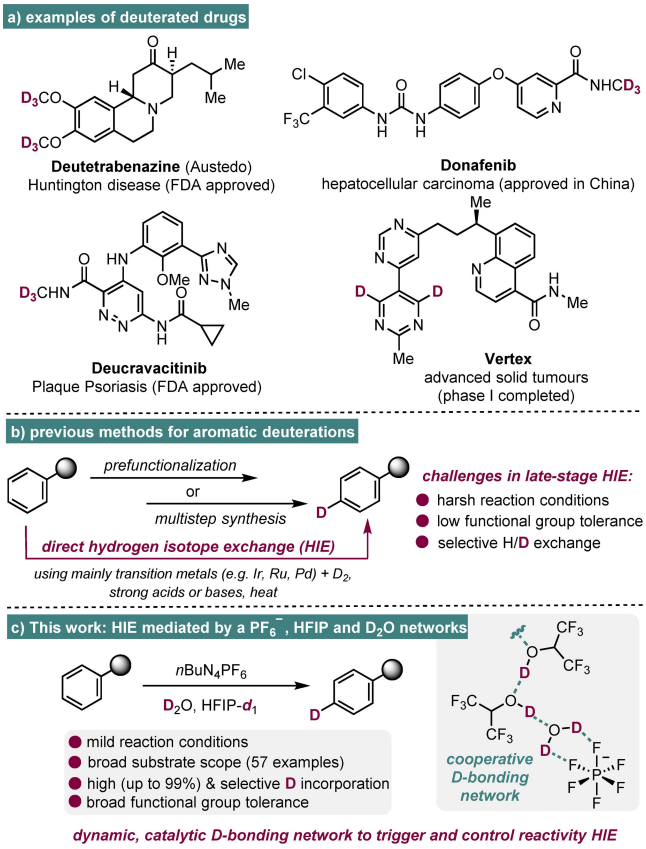

Figure 1. Background and current methods for aromatic deuterations using HIE.

Lewis acids[12] and bases (Figure 1b).[13] The process of labeling arenes using acid-mediated H/D exchange has a long history. However, it only permits the selective introduction of deuterium into simple substrates. Most existing protocols employ high temperatures and excess strong acids like concentrated H_2SO_4 or HCl. This results in low functional group tolerance and safety concerns, mainly when used on a larger scale.[14] Transition metal catalysts, such as Ir, Pd, or Rh, in combination with D_2, offer an alternative pathway.[14a,15] Substrates suitable for this strategy must exhibit a specific substitution pattern or explicitly introduce directing groups. This, together with harsh reaction conditions to facilitate deuteration, hampers the broad applicability of this process. Despite its recent progress, implementing HIE as a standard tool in synthetic laboratories remains an active but challenging research area. HIE's current obstacles must be overcome first, and operationally simple methods with a broader functional group tolerance, higher and more selective deuterium incorporation under milder conditions, and readily available and cheap labeling reagents and catalysts/mediators must be established. First attempts in this direction have recently been reported employing photocatalytic[10a,c,16] and electrochemical[10e,17] methods. These approaches have the advantage of utilizing readily available starting materials, their affordability, and the high atom economy aligning with the principles of green chemistry.

This article presents the application of a unique anion-water-F-alcohol assembly for the general and efficient deuteration of arenes and heteroarenes (Figure 1c). By utilizing D_2O with a catalytic amount of simple hexafluorophosphate salts under ambient conditions, producing >50 deuterated building blocks, drug, and natural-product derivatives with consistently high deuterium incorporation is feasible. The unique deuterium-bonding network and the thus triggered reaction mechanism were studied at the molecular level employing spectroscopic and theoretical methods, shedding new light on the underlying principles of solvent-solute interactions and how this can be harnessed for the activation of the strong P–F bond in hexafluorophosphate facilitating reactions in microstructured solutions.

Results and Discussion

Encouraged by the latest results in the electrochemical HIE reaction of pyridine derivatives,[17c,e] we initially aimed to further extend the electrochemical toolbox to benzene derivatives. We started our investigations using 2-methyl phenol (**1a**) as the model substrate, nBu$_4$NPF$_6$ as the electrolyte, and D_2O (10 equiv.) as a deuterium donor. As the solvent, we employed hexafluoropropan-2-ol-d_1 (HFIP-d_1) because F-alcohols proved to be an advantageous medium in electrochemical transformations of aryls, as demonstrated for biaryl couplings.[18] After electrolyzing the reaction mixture at 3.0 mA constant current in an undivided cell for 4 hours at room temperature (Table 1, entry 1), we observed H/D exchange at the *ortho*- and *para*-positions, giving the deuterated phenol *d*-**1a** with a 60 % deuterium incorporation and 31 % yield. Before further optimizing our electrochemical conditions, we conducted control experiments, omitting each component of the reaction mixture in turn (Table 1 entries 2 and 3 and Supporting Information). No deuteration was visible when running the reaction without electricity for 4 hours (Table 1, entry 2). But to our surprise, by further extending the reaction time to 24 hours (Table 1, entry 3), we obtained the deuterated cresol (*d*-**1a**) even with an increased D % (83 %) and 97 % yield. This unexpected outcome, which significantly improved deuterium incorporation and yield, sparked our interest in further elaborating on this transformation and understanding the factors causing this phenomenon to establish an efficient and cost-effective method for selective hydrogen isotope exchange.

We systematically screened reaction conditions (Table 1, entries 4–15 and Supporting Information). The best combination included catalytic amounts of nBu$_4$PF$_6$ (30 mol %), 6 eq. D_2O in HFIP-d_1 yielded the deuterated phenol *d*-**1a** with 97 % and 93 % deuterium incorporation (Table 1, entry 4). Fluorinated solvents played a decisive role in this HIE reaction. The corresponding non-fluorinated solvents (entry 5, Supporting Information) did not deliver *d*-**1a**. HFIP-d_1 outperformed other fluorinated solvents, such as trifluoroethanol-d_1 (TFE-d_1, entry 6) or perfluoro-*t*-butanol-

Table 1: Initial Screening of Electrochemical HIE[a,b]

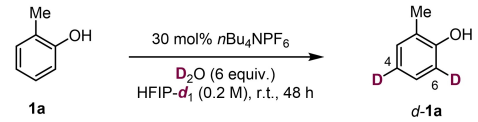

1a d-1a

entry	Changes made to standard conditions	Yield *d*-**1a** [%][c]	4/6 [D %][d]
1[a]	C(+)|C(−), 3.0 mA, nBu_4NPF_6 (10 equiv.), D_2O (10 equiv.) undivided cell, 4 h	31	60/60
2[b]	nBu_4NPF_6 (10 equiv.), D_2O (10 equiv.) undivided cell, 4 h	–	0/0
3[b]	nBu_4NPF_6 (10 equiv.), D_2O (10 equiv.) undivided cell, 24 h	97	83/83
4[b]	none	97	93/93
5[b]	*i*PrOD instead of HFIP-d_1	n.d.	0/0
6[b]	TFE-d_1 instead of HFIP-d_1	98	21/21
7[b]	No D_2O	n.d.	0/0
8[b]	No HFIP-d_1	n.d.	0/0
9[b]	H_2O instead of D_2O	n.d.	<5%
10[b]	HFIP instead of HFIP-d_1	n.d.	22/22
11[b]	Me_4NPF_6 instead of nBu_4NPF_6	97	88/88
12[b]	Ph_3CPF_6 instead of nBu_4NPF_6	94	90/90
13[b]	$AgPF_6$ instead of nBu_4NPF_6	84	88/88
14[b]	nBu_4NCl instead of nBu_4NPF_6	n.d.	0/0
15[b]	nBu_4NBF_4 instead of nBu_4NPF_6	n.d.	0/0

[a] Electrochemical reactions were performed with **1a** (0.2 mmol), nBu_4NPF_6 (0.2 mmol), D_2O (2.0 mmol), and HFIP-d_1 (1.0 mL) with two graphite electrodes, constant current electrolysis (I = 3.0 mA) in an IKA glassware for 4 h. [b] Reactions were performed with **1a** (0.1 mmol), salt (0.03 mmol), D_2O (0.6 mmol) in 0.5 mL of solvent in for 48 h. [c] yields were determined by ^{1}H NMR spectroscopy of the crude reaction mixture using 1,3,5-trimethoxybenzene as internal standard. [d] Deuterium incorporation was determined by ^{1}H NMR spectroscopy.

d_1 (see Supporting Information, Table S2), hinting at a decisive impact of the deuterium bonding network induced by HFIP-d_1.[19] Applying a defined ratio of HFIP and water was crucial for a successful transformation (see Supporting Information). Omitting one of the components led to no conversion (Table 1, entries 7 and 8). D-incorporation reached its maximum (93 %) when 6 eq. D_2O was employed in a 0.2 M HFIP-d_1 solution. Increasing and decreasing the D_2O concentration resulted in a lower deuteration grade of **1a** (cf. Supporting Information, Table S5).

Substituting either HFIP-d_1 or D_2O with their hydrogen derivatives led to a considerable reduction or non-deuterium incorporation (22 D % and 0 D %, respectively; Table 1, entries 9 and 10). These results are attributed to the rapid exchange of deuterium and hydrogen atoms between HFIP and water and, thus, an overall depletion of the deuterium content in the reaction mixture. Furthermore, the transformation was restricted to hexafluorophosphate salts regardless of their accompanying cation (Table 1, entries 11–13, Supporting Information, Table S4). Surprisingly, more reactive and nucleophilic anions, such as chloride and tetrafluoroborate, did not trigger the transformation (Table 1, entries 14 and 15, Supporting Information). The reaction only succeeded when D_2O was used as a deuterium donor with catalytic PF_6 salts in HFIP.

After determining the optimal reaction conditions, we investigated the scope of this HIE reaction. Encouragingly, a wide variety of phenols **1** and anisoles **2** with different electronic and steric substitution patterns, like, e.g., alkyl, aldehyde, nitrile, and ester functionalities or halogen atoms, could be converted (Scheme 1). The resulting deuterated products *d*-**1a**–*d*-**1q** and *d*-**2a**–*d*-**2i** overall showed excellent yields (80–99 %) and high levels of deuterium incorporation *ortho* and *para* to the hydroxy functionality (up to 96 D %). While 30 mol % PF_6 salt was necessary to obtain the isotopically labeled compounds *d*-**1**, the catalyst loading could be reduced to 10 mol % when anisoles **2** served as substrates. It

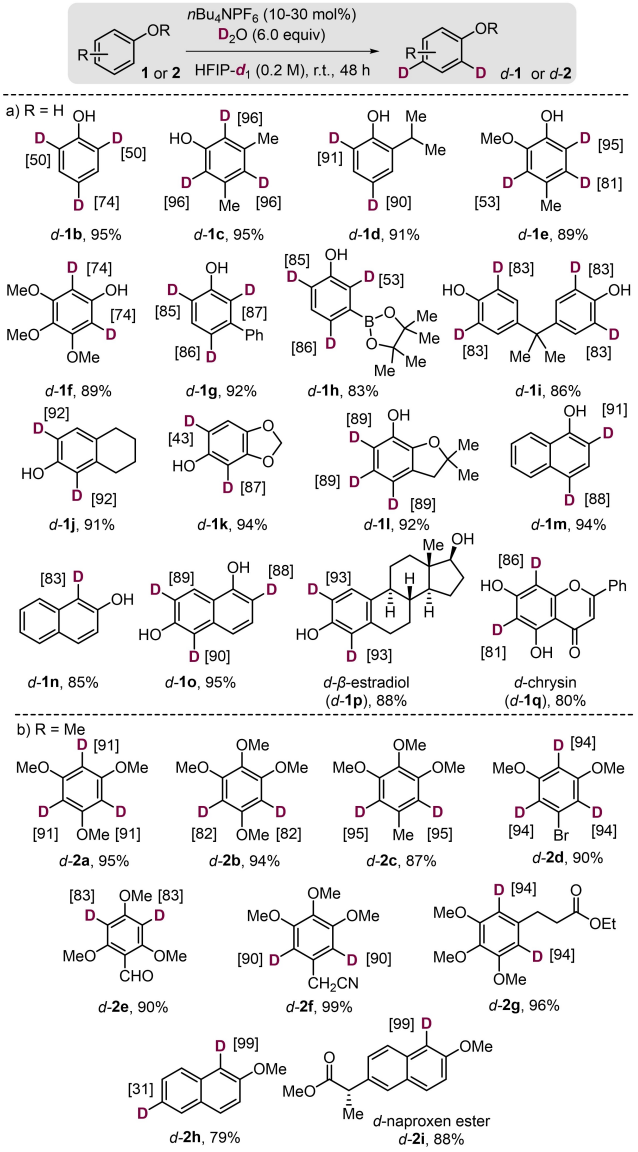

Scheme 1. Substrate scope for the nBu_4NPF_6 catalyzed HIE reaction of a) phenol **1** and b) anisole **2** derivatives. All reactions were performed with **1** or **2** (0.2 mmol), nBu_4NPF_6 (10–30 mol %), and D_2O (1.2 mmol) in 1.0 mL of HFIP-d_1 for 48 h. 0.06 mmol and 0.02 mmol nBu_4NPF_6 were used for substrates **1** and substrates **2**, respectively. Deuterium incorporation was determined by ^{1}H NMR spectroscopy. All yields refer to isolated material.

is noteworthy that the mild reaction conditions also allowed the efficient conversion of chemically sensitive and structurally complex molecules, such as naphthol derivatives *d*-**1m**–*d*-**1o**, 2-methoxynaphthalene (*d*-**2h**), and the naproxen ester *d*-**2i** as well as the natural products estradiol (*d*-**1p**) and chrysin (*d*-**1q**). In the latter case, only the more electron-rich phenol moiety showed deuterium incorporation, leaving the non-substituted phenyl ring untouched.

The promising results achieved for the HIE of phenols **1** and anisoles **2** motivated us to investigate the feasibility of applying the same method to other aromatic compounds. The established platform proved likewise effective for various substituted anilines **3** (Scheme 2), producing the corresponding products *d*-**3a**–*d*-**3l** with up to 94 D %. H–D exchange was restricted to the aryl portion. Other C–H bonds were not affected by isotope exchange. For example, alkene moieties (→*d*-**3h**), as well as allyl (→*d*-**3h**) and benzyl (→*d*-**3i**) positions, which are prone to HIE exchange using standard conditions, did not react.

Furthermore, we transferred our newly established H/D-exchange platform to heterocyclic compounds, given their importance and thus widespread presence in drugs (Scheme 3). Switching the alkyl portion of the ammonium salt from *n*Bu to Me was necessary to achieve a good turnover of substrates **4**. Testing various indoles exhibiting different substituents at the nitrogen and the aryl ring provided the corresponding products *d*-**4a**–*d*-**4h** mostly solely deuterated at C-3 when 10 mol % of Me_4NPF_6 was employed. Only for the 2-Me indoles, *d*-**4g**, and *d*-**4h** deuterium implementation at the benzylic position was observed, while all other substrates bearing benzylic positions did not show such behavior. When the 3-position is blocked (→*d*-**4i** and *d*-**4j**), the HIE happened at C-2 with

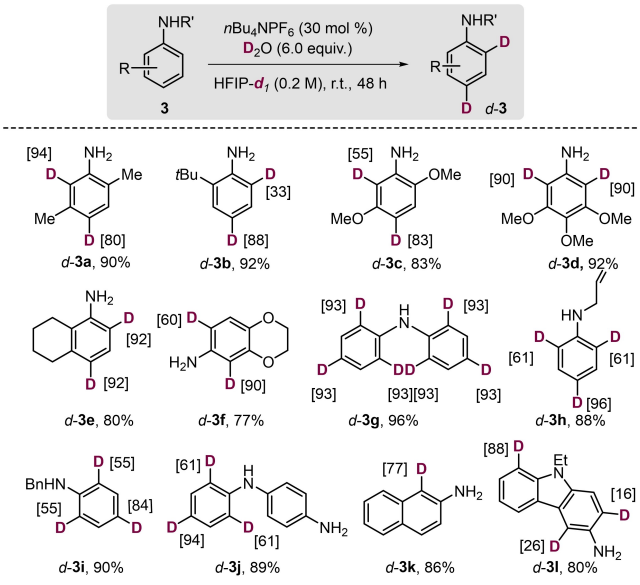

Scheme 2. Substrate scope for the nBu_4NPF_6 catalyzed HIE reaction of anilines **3**. All reactions were performed with **3** (0.2 mmol), nBu_4NPF_6 (0.06 mmol), and D_2O (1.2 mmol) in 1.0 mL of HFIP-d_1 for 48 h. Deuterium incorporation was determined by ^{1}H NMR spectroscopy. All yields refer to isolated materials.

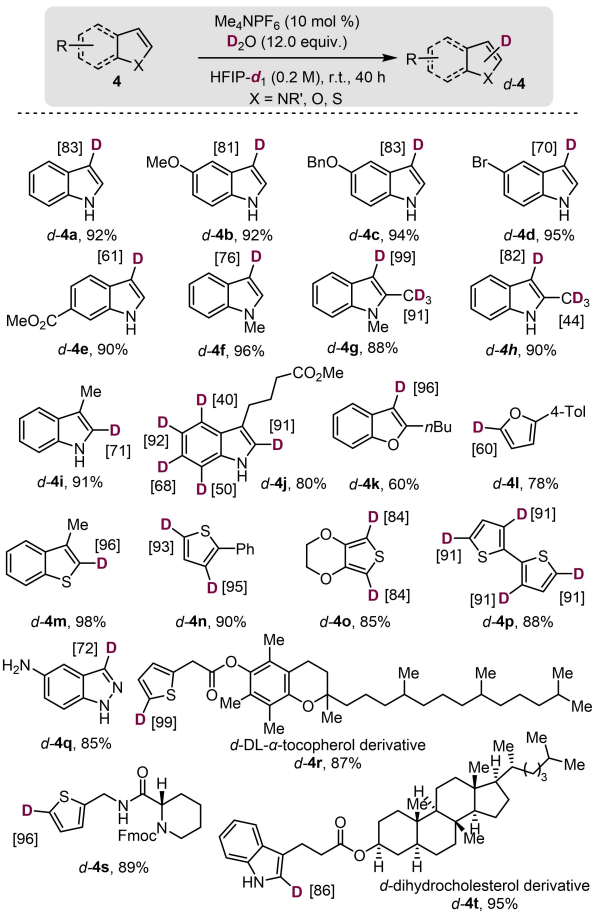

Scheme 3. Substrate scope for the nBu_4NPF_6 catalyzed HIE reaction of heterocycles 4. All reactions were performed with 4 (0.2 mmol), Me_4NPF_6 (0.02 mmol), and D_2O (1.2 mmol) in 1.0 mL of HFIP-d_1 for 40 h. Deuterium incorporation was determined by ^{1}H NMR spectroscopy. All yields refer to isolated materials.

71 D % and 91 D %, respectively. Other electron-rich heterocyclic compounds, like, e.g., furans *d*-**4k** and *d*-**4l**, thiophenes *d*-**4m**–*d*-**4p**, and indazoles *d*-**4q** were likewise suitable as substrates and showed deuterium incorporations of up to 96 D %. A plethora of functional groups were tolerated, showcased i.a., by structurally complex, natural-product derived compounds, such as the tocopherol *d*-**4r** (99 D %), the pipecolic acid *d*-**4s** (96 D %), and the dihydrocholesterol derivative *d*-**4t** (86 D %). In all cases, no erosion of the enantiomeric purity was detectable.

Puzzled by the observed reactivity, we started to elucidate the underlying principles of the HIE reaction and conducted a series of experiments to investigate its mechanism. First, we determined the time course of the D incorporation in **1a** by NMR spectroscopy (Figure 2b). There, we observed an onset time for the HIE of 9 hours, followed by a rapid turnover of our substrate **1a** within the next 13 hours. This outcome was in line with our observation that no deuterated product *d*-**1a** was formed in 4 hours of reaction time (cf. Table 1). Detailed NMR studies on the decisive mixture of HFIP, H_2O, and nBu_4NPF_6 revealed the formation of a new species at the same time D incorporation

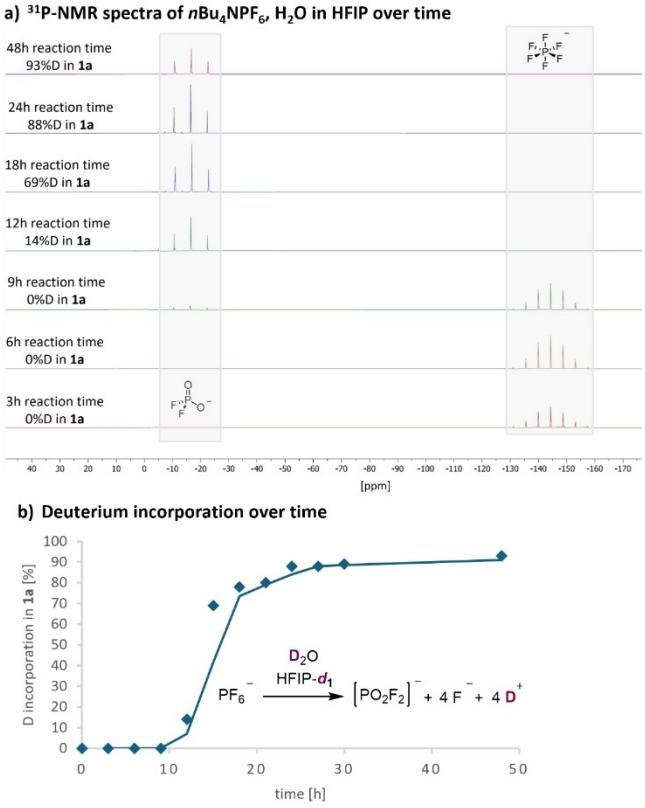

Figure 2. NMR investigations on the HIE reaction of **1a**.

started (9 hours), which occurred as a triplet at −16.69 ppm in the ^{31}P NMR spectrum (Figure 2a, for the ^{19}F NMR spectra, see Supporting Information, Figure S8). This signal increased over time at the expense of the PF_6^- signal (−144.4 ppm). The same signal was found in the NMR spectra of the reaction mixture after 9 hours (see Supporting Information), suggesting an essential role in the deuteration reaction. The new compound was identified as difluorophosphate $PO_2F_2^-$, usually formed together with HF/DF upon hydrolysis of POF_3 (see Supporting Information, Figure S4). The formation of DPO_2F_2 was further corroborated by a decrease in pH over time (see Supporting Information, chapter 7 for details). In contrast, hexafluorophosphate is known as a non-nucleophilic, chemically inert anion, resulting in its widespread application as an 'innocent' anion, i.e., in inorganic complexes[20] or as an electrolyte in electrochemical reactions.[21] Usually, hydrolysis of the strong P–F bond in PF_6^- occurs only under harsh conditions, such as high temperature or high pressure.[22] Even in strongly alkaline (pH > 12) and acidic (pH < 1) solutions, PF_6^- remains chemically stable.[22a,23] Hydrolysis of PF_6^- has primarily been reported in batteries,[21] in polypropylene carbonate/dimethyl carbonate mixtures, and during the reaction of $[Pd(\eta3\text{-}2\text{-}Me\text{-}C_3H_4)](\mu\text{-}Cl)]_2$ with $AgPF_6$.[23] Therefore, the formation of HPO_2F_2 under these mild reaction conditions and occurring only in HFIP-water mixtures was surprising and warranted further investigation.

To elucidate the role of the different F-containing hydrolysis products DPO_2F_2 and DF on the HIE, we directly replaced nBu_4NPF_6 with HF and HPO_2F_2, respectively (Table 2 and Supporting Information). When 1.0 or 5.0 equivalent of $3HF\cdot Et_3N$ were used, no deuterated product *d*-**1a** was obtained (Table 2, entries 1 and 2), indicating that HF/DF is not the driving force of the reaction. Adding the lithium and ammonium PO_2F_2 salts did not convert **1a** (Table 2, entries 3 and 4, Supporting Information). However, switching from the salts to the corresponding acid HPO_2F_2 resulted in significant deuterium incorporation of 60 % and 82 % if 30 mol % acid was used (Table 2, entry 5). The H/D exchange was further enhanced by increasing the amount of HPO_2F_2 (Table 2, entry 6). These findings strongly support the pivotal role of DPO_2F_2 in driving the hydrogen isotope exchange reaction. Interestingly, when MeOD was used as a solvent, no deuterated product *d*-**1a** was produced (Table 2, entry 7). This observation underscores the essential role of HFIP not only for the activation of PF_6^- towards hydrolysis, producing HPO_2F_2, but also for facilitating the electrophilic aromatic substitution (S_EAr), leading to the deuterium incorporation in aryl moieties.

In the next step, we looked closer at the PF_6^-, water, and HFIP mixture, elucidating the activation of the chemically stable hexafluorophosphate to its hydrolysis. Revealing the interplay of PF_6^- and HFIP is a crucial step toward understanding the role of HFIP in the nucleophilic addition of water to PF_6^-. ^{1}H NMR spectra obtained from the titration of nBu_4NPF_6 with HFIP showed a significant downfield shift and signal broadening of the hydroxy-proton signal of the fluoro alcohol from 3.17 ppm to 4.06 ppm (Figure 3). At the same time, the NCH_2 groups of the *n*Bu moieties were only slightly affected by the addition of HFIP. This strongly indicates a non-covalent interaction between the F-alcohol and the anion.

Complementary experimental information on the nature of the hydrogen bonds formed by solvating PF_6^- with HFIP in the presence of H_2O was obtained by ion vibrational spectroscopy on microsolvated PF_6^- complexes isolated in the gas phase. This technique allows probing the hydrogen bond strength in ion-solvent complexes by measuring the

Table 2: Screening of different PF_6^- hydrolysis products as additives in the HIE reaction of cresol (**1a**)[a]

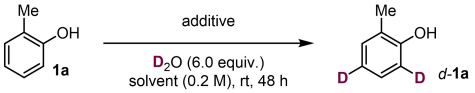

entry	additive	solvent	4/6 [D%][d]
1	HF NEt_3 (1 eq.)	HFIP-d_1	0/0
2	HF NEt_3 (5 eq.)	HFIP-d_1	0/0
3	$LiPO_2F_2$ (5 eq.)	HFIP-d_1	0/0
4	$nBu_4NPO_2F_2$ (5 eq.)	HFIP-d_1	0/0
5	HPO_2F_2 (30 mol %)	HFIP-d_1	60/82
6	HPO_2F_2 (5 eq.)	HFIP-d_1	85/85
7	HPO_2F_2 (5 eq.)	MeOD	0/0

[a] 2-Methylphenol (**1a**, 0.10 mmol, 10.8 mg), additive, D_2O (0.60 mmol, 12.0 mg, 6 eq.) in 0.50 mL HFIP-d_1 was stirred at rt for 48 h. [b] Deuterium incorporation was determined by ^{1}H NMR spectroscopy.

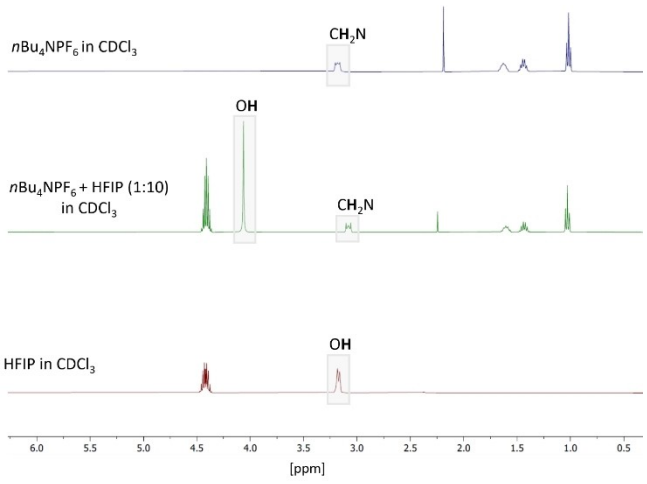

Figure 3. Overlay of the ^{1}H NMR spectra of nBu$_4$NPF$_6$, nBu$_4$NPF$_6$, and HFIP (1 : 10), and HFIP in $CDCl_3$ at 25 °C

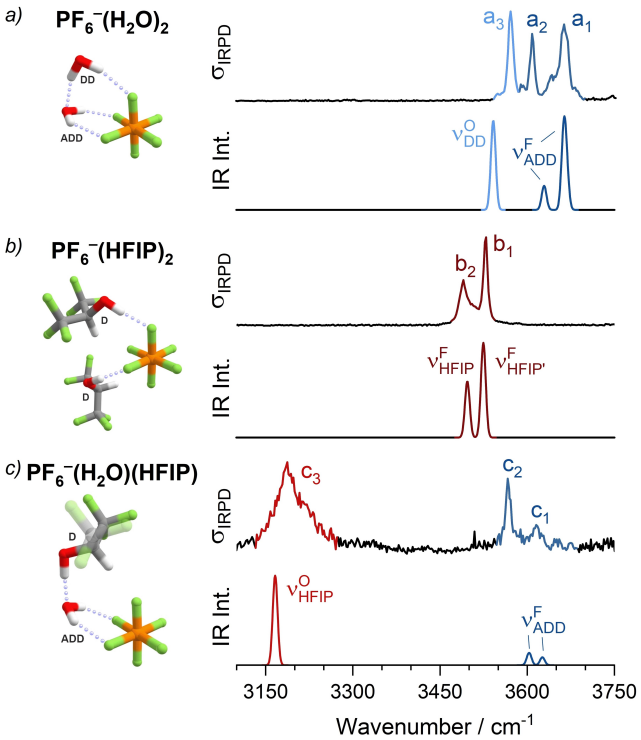

Figure 4. DFT minimum-energy structures of the lowest energy isomer (left) and vibrational spectra in the O–H stretching region (right) for $PF_6^-(H_2O)_2$ (a), $PF_6^-(HFIP)_2$ (b), and $PF_6^-(H_2O)(HFIP)$ (c). Each solvent molecule is labeled according to the number of interactions between hydrogen-bond donor (D) and acceptor (A). Only OH···F hydrogen bonds (D) are considered. For each system, the IRPD spectrum (top) is compared to the simulated IR spectrum (bottom). All observed features are assigned to stretching modes of O–H moieties (see Table S13 in the Supporting Information for band position, harmonic frequencies, and assignments) involved in either ionic (H_2O/anion: dark blue, HFIP/anion: dark red) or intermolecular (H_2O/H_2O: blue, HFIP/water: red) hydrogen bonds. See Supporting Information (Section 12) for details of the methods used.

redshift $\Delta\nu_{OH}$ induced in the corresponding OH stretching frequency. In the following, we use the PF_6^- anion interacting with two solvent molecules as a simple model system to qualitatively assess the relative strength of the solute-solvent vs. the solvent-solvent interactions and how the onset of hydrogen-bond network formation affects these interactions.

The vibrational spectra of $PF_6^-(H_2O)_2$, $PF_6^-(HFIP)_2$, and $PF_6^-(H_2O)(HFIP)$ in the OH stretching region, measured by way of infrared photodissociation (IRPD) spectroscopy of the corresponding D_2-tagged species (see Supporting Information for experimental details), are shown in Figure 4 (see Table S13 for band positions, redshifts, and assignments). No bands are observed above 3700 cm^{-1}, indicating that no free OH oscillators are present in these systems. For the pure solvent anion complexes, $PF_6^-(H_2O)_2$ and $PF_6^-(HFIP)_2$, we observe OH stretching bands (labeled a_{1-3} and b_{1-2} in Figure 4) exclusively in the spectral range above 3490 cm^{-1}. The associated redshifts, ranging from 44 cm^{-1} to 166 cm^{-1} (see Table S13), are moderate, indicating the presence of exclusively weaker hydrogen bonds, as is expected for the microsolvation of a weakly coordinating anion like PF_6^-.[24] For the mixed solvent complex $PF_6^-(H_2O)(HFIP)$, in contrast, the substantially more redshifted OH stretching band (labeled c_3 in Figure 4c) at 3166 cm^{-1}, corresponding to a redshift of 438 cm^{-1}, suggest that unexpected synergistic effects are at play when both solvent molecules are present.

To identify the origin of this characteristically redshifted OH stretching band, we performed density functional theory (DFT) calculations (see Section 12 of the Supporting Information for computational details and an overview of the computational results). These provided us with minimum-energy structures of the lowest-energy isomers and the corresponding simulated IR spectra, which are both also shown in Figure 4. The agreement between the (experimental) IRPD and DFT IR spectra is satisfactory, supporting our structure assignment (see Figure S12 for the predicted IR spectra of other isomers). The stability of the identified structures (see Figure 4) can be rationalized by considering the hydrogen bond donor (D) and acceptor (A) interactions of the solvent molecules. For example, H_2O can bind to PF_6^- in a double donor (DD) fashion, while HFIP exhibits only a single significant HB donor, which binds stronger to PF_6^- than either of the two OH groups in H_2O. This is a consequence of HFIP's higher gas-phase acidity. $PF_6^-(HFIP)_2$ (see Figure 4b) exhibits a structure in which each HFIP molecule exclusively donates a hydrogen bond to the anion, forming two ionic hydrogen bonds. In contrast, $PF_6^-(H_2O)_2$ consists of one ADD- and one DD-H_2O molecule that forms an intermolecular hydrogen bond in addition to three ionic hydrogen bonds. Irrespective of these structural differences, the observed redshifts are smaller than 170 cm^{-1}, indicating that hydrogen bonding in both systems is weak.

The structure identified for the mixed-solvent complex (Figure 4c) is different and unexpected. $PF_6^-(H_2O)(HFIP)$ contains an ADD-H_2O, i.e., the water molecule binds to PF_6^- in a double donor fashion, but HFIP now predominantly interacts with the H_2O molecule and not with the

anion. The driving force is the formation of a strong intermolecular (vs. ionic) hydrogen bond, evidenced by the marked redshift of band c_3 (see Figure 4c). This hydrogen bond is the strongest and, hence, the shortest in all three systems studied here (see Figure S10). It is predicted to be 20 % shorter than the intermolecular hydrogen bond in $PF_6^-(H_2O)_2$ and even 5 % shorter than the ionic hydrogen bonds in $PF_6^-(HFIP)_2$. Moreover, stronger intermolecular hydrogen bonding also leads to a more substantial activation of the ADD-H_2O, compared to $PF_6^-(H_2O)_2$, evidenced by the more redshifted pair of bands b_1 and b_2 vs. a_1 and a_2 in Figure 4. This shift translates into 5 % shorter ionic hydrogen bonds when HFIP replaces the DD-H_2O. In other words, substituting a water molecule with an HFIP molecule strengthens the directly involved intermolecular hydrogen bond and affects the more remote anion-water interaction.

The effects observed in the present gas phase experiments (performed at cryogenic temperatures) are small, and the insights obtained are not directly transferable to solution phase experiments at room temperature. However, they do suggest that whenever HFIP and water are present at the same time, either in the gas or the solution phase, HFIP's more pronounced hydrogen-bond donation ability may lead to a preference for activating a water molecule in PF_6^-'s first solvation shell over directly interacting with the anion itself. This effect, not present in the respective clean solvents, may contribute to enabling the above-described hydrolysis reaction in a way that is not unlike the previously reported increase in catalytic activity due to the microstructuring of reaction mixtures.[19c–f]

Ultimately, the hydrolysis of PF_6^- observed only in F-alcohols is likely the result of a kinetic effect. We thus investigated the influence of HFIP on the thermodynamics and the reaction barrier for the hydrolysis of PF_6^- at the ωB97x-D3BJ/def2-TZVP level.[25] Beyond the microsolvation approach outlined below, we considered the electrostatic influence of the solvent in the solution chemistry approach via a conductor-like polarizable continuum model (CPCM).[26] Our focus was the influence of the number of HFIP molecules on the Gibbs energy (ΔG) and the reaction barrier ($\Delta G^{\ddagger}$) for eq. (1).

$$PF_6^- + 2\,H_2O + n\,HFIP \longrightarrow [PO_2F_2]^- + 4\,HF + n\,HFIP \quad \text{with n=0,1,3} \quad (1)$$

First, we analyzed the influence of HFIP on ΔG. While the hydrolysis reaction without HFIP is endergonic ($\Delta G_{n=0} = 37\ kJ\,mol^{-1}$), and the addition of one HFIP molecule only gives a marginal gain ($\Delta G_{n=1} = 24\ kJ\,mol^{-1}$), the consideration of three HFIP molecules leads to an exergonic reaction ($\Delta G_{n=3} = -14\ kJ\,mol^{-1}$). This is the first indication of the strong influence on the hydrolysis reaction.

More relevant for the observed reactivity is the influence on the barrier for the hydrolysis reaction, where we assume the first reaction step is rate-determining. The barriers for this reaction step ($PF_6^- + H_2O + n$ HFIP→$PF_2OH^- + HF +$ n HFIP) are thus shown in Figure 5 for different numbers ($n = 0$, 1, 3, 4) of HFIP molecules considered in the calculations. All structures of reactants, transition state, and product are shown in the Supporting Information (Figure S12).

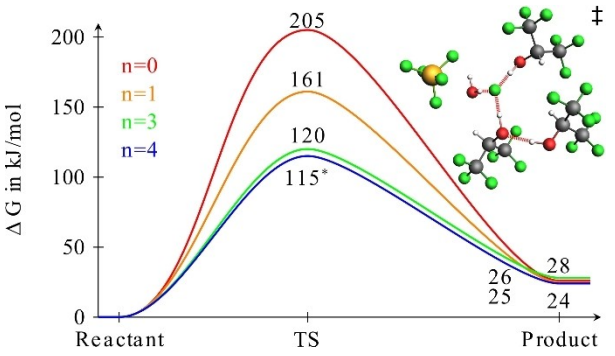

Figure 5. Schematic representation of the energy profiles for the first reaction step of the hydrolysis of PF_6^- ($PF_6\ H_2O + n$ HFIP→$PF_2OH^- + HF + n$ HFIP) with a different number ($n = 0$ (red), 1 (orange), 3 (green), 4 (blue)) of considered HFIP molecules. Energies for TS ($\Delta G^{\ddagger}$) and product (ΔG) are given in kJ mol^{-1} relative to the energies of the respective reactants. The TS structure for $n = 3$ is shown. Thereby, the barrier for $n = 4$ is estimated (indicated by an asterisk) as discussed in more detail in the Supporting Information.

Figure 5 shows that the reaction's Gibbs energy for the first hydrolysis step is hardly changed by the number of HFIP molecules ($\Delta G = 24$–$28\ kJ\,mol^{-1}$). The barrier, however, shows a powerful influence. While we have a huge barrier of $\Delta G^{\ddagger} = 205\ kJ\,mol^{-1}$ for the reaction without HFIP (red curve, Figure 5), this is lowered by $44\ kJ\,mol^{-1}$ by the addition of one HFIP molecule (orange curve, Figure 5) and by a further $41\ kJ\,mol^{-1}$ if we consider three HFIP molecules (green curve, Figure 5). The HFIP trimer has previously been found to be an essential structural motif in liquid HFIP.[27] After carefully analyzing the transition state structure for this molecule (see Supporting Information, Figure S12), it became clear that stabilizing the fluoride anion at the transition state via hydrogen bonding is crucial. We could also identify an empty coordination site for the structure with three HFIP molecules. Consequently, adding a fourth HFIP molecule to this coordination site leads to a tetrahedrally coordinated F^- anion at the transition state (for the HFIP trimer), additionally strengthening one hydrogen bond via an additional HFIP molecule in the second solvation shell. This results in a barrier approximately half as large as the implicit solvated case with $\Delta E^{\ddagger} = 115\ kJ\,mol^{-1}$ (blue curve, Figure 5). Due to convergence issues, only the electronic energy barrier is obtained for this system. This is an upper bound to the barrier since $\Delta G^{\ddagger}$ is consistently lower by 1–12 $kJ\,mol^{-1}$ for $n = 0$–3 (table S12). This is well in the energy range, which can be overcome experimentally at room temperature. Thus, it explains the unusual observation of PF_6^- hydrolysis at room temperature in an HFIP solution.

Conclusion

A versatile, user-friendly, robust, and mild approach has been developed for the HIE reaction of electron-rich compounds. Phenols, anilines, anisoles, and heterocyclic

compounds exhibiting a plethora of functional groups are compatible reaction partners in this protocol, allowing access to a broad range of synthetically and biologically valuable deuterated (hetero)aromatic compounds in high yields and excellent deuteration incorporation levels. In-depth mechanistic investigations revealed an unusually high reactivity of hexafluorophosphate toward the nucleophilic attack of water, producing in situ DPO_2F_2 that acts as the actual deuteration reagent. As this transformation can only occur within the distinct fluorinated alcohols with HFIP performing best, extended studies on the influence of the H-bonding network stemming from water-HFIP mixtures and their effect on the reactivity have been undertaken. Thereby, IRPD spectroscopy showed a significant strengthening of the water-PF_6^- interaction in the presence of HFIP. Similar interactions were previously documented for causing enhanced catalytic activity, e.g., terpene cyclizations or epoxide openings. Here, the observed effect, which is absent in the pure solvents, could facilitate the hydrolysis of PF_6^-. Computational studies, however, identified that stabilizing the fluoride anion in the transition state of the hydrolysis step via hydrogen bonding is essential for the observed reactivity. The kinetic barrier of the attack of the first water molecule to the electrophilic phosphor atom is substantially reduced by HFIP. Interestingly, cooperative hydrogen bonds of up to four HFIP molecules in the first and second solvation shells around the fluoride anion within the complex H/D-bonding network are needed to activate the strong P–F bond and thus trigger the reaction at room temperature. Activating strong bonds in general, particularly under ambient conditions, is yet an unmatched challenge for organic chemists. Therefore, the insights into the fundamental principles of H-bonding networks in microstructured, fluorinated environments, as shown in this study, will not only contribute to further enhancements in deuterium incorporation processes but also pave the way for a general application of such F-alcohol assemblies in the activation of strong bond processes.

Supporting Information

The authors have cited additional references within the Supporting Information.[28–41]

Acknowledgments

We thank Daniel Wegener, FU Berlin, for providing NMR spectra of POF_3 and valuable scientific discussions. Financial support of the Deutsche Forschungsgemeinschaft (DFG)—Project-ID 443871192—GRK 2721: "Hydrogen Isotopes 123H" is gratefully acknowledged. Y. N. thanks the Chinese Scholarship Council for a PhD Fellowship. T. G. thanks the International Isotope Society—Central European Division and the PharmaScienceHub (PSH) for their support. Open Access funding enabled and organized by Projekt DEAL.

Conflict of Interest

The authors declare no conflict of interest.

Data Availability Statement

The data that support the findings of this study are available in the supplementary material of this article.

Keywords: deuterium · 1,1,1,3,3,3-hexafluoroisopropanol · ion vibrational spectroscopy · computational chemistry · hydrogen bonding cluster

[1] a) J. Atzrodt, V. Derdau, T. Fey, J. Zimmermann, *Angew. Chem. Int. Ed.* **2007**, *46*, 7744–7765; b) S. Kopf, F. Bourriquen, W. Li, H. Neumann, K. Junge, M. Beller, *Chem. Rev.* **2022**, *122*, 6634–6718.
[2] a) T. Pirali, M. Serafini, S. Cargnin, A. A. Genazzani, *J. Med. Chem.* **2019**, *62*, 5276–5297; b) R. M. C. Di Martino, B. D. Maxwell, T. Pirali, *Nat. Rev. Drug Discov.* **2023**, *22*, 562–584; c) A. Sib, V. Derdau, *Synlett* **2024**, doi.10.1055/a-2222-1667; d) J. Atzrodt, V. Derdau, W. J. Kerr, M. Reid, *Angew. Chem. Int. Ed.* **2018**, *57*, 3022–3047; e) J. Atzrodt, V. Derdau, W. J. Kerr, M. Reid, *Angew. Chem. Int. Ed.* **2018**, *57*, 1758–1784.
[3] K. Müller, A. Seubert, *Isotop. Environment. Health Stud.* **2014**, *50*, 88–93.
[4] G. Prakash, N. Paul, G. A. Oliver, D. B. Werz, D. Maiti, *Chem. Soc. Rev.* **2022**, *51*, 3123–3163.
[5] E. M. Simmons, J. F. Hartwig, *Angew. Chem. Int. Ed.* **2012**, *51*, 3066–3072.
[6] Y. Li, Q. Meng, M. Yang, D. Liu, X. Hou, L. Tang, X. Wang, Y. Lyu, X. Chen, K. Liu, A. M. Yu, Z. Zuo, H. Bi, *Acta Pharm. Sin.* **2019**, *9*, 1113–1144.
[7] a) C. Elison, H. Rapoport, R. Laursen, H. W. Elliott, *Science* **1961**, *134*, 1078–1079; b) B. Belleau, J. Burba, M. Pindell, J. Reiffenstein, *Science* **1961**, *133*, 102–104.
[8] a) S. H. DeWitt, B. E. Maryanoff, *Biochem.* **2018**, *57*, 472–473; b) C. Schmidt, *Nat. Biotechnol.* **2017**, *35*, 493–494.
[9] a) K. Sanderson, *Nature* **2009**, *458*, 269; b) A. Katsnelson, *Nat. Med.* **2013**, *19*, 656–656.
[10] a) C. Liu, Z. Chen, C. Su, X. Zhao, Q. Gao, G.-H. Ning, H. Zhu, W. Tang, K. Leng, W. Fu, B. Tian, X. Peng, J. Li, Q.-H. Xu, W. Zhou, K. P. Loh, *Nat. Commun.* **2018**, *9*, 80; b) C. Liu, S. Han, M. Li, X. Chong, B. Zhang, *Angew. Chem. Int. Ed.* **2020**, *59*, 18527–18531; c) Y. Li, Z. Ye, Y.-M. Lin, Y. Liu, Y. Zhang, L. Gong, *Nat. Commun.* **2021**, *12*, 2894; d) J. L. Koniarczyk, D. Hesk, A. Overgard, I. W. Davies, A. McNally, *J. Am. Chem. Soc.* **2018**, *140*, 1990–1993; e) D. Wood, S. Lin, *Angew. Chem. Int. Ed.* **2023**, *62*, e202218858.
[11] T. Junk, W. J. Catallo, *Chem. Rev.* **1997**, *26*, 401–406.
[12] a) J. L. Garnett, M. A. Long, R. F. W. Vining, T. Mole, *J. Am. Chem. Soc.* **1972**, *94*, 5913–5914; b) M. A. Long, J. L. Garnett, R. F. W. Vining, *J. Chem. Soc. Perkin Trans. 2* **1975**, 1298–1303; c) M. H. G. Prechtl, M. Teltewskoi, A. Dimitrov, E. Kemnitz, T. Braun, *Chem. Eur. J.* **2011**, *17*, 14385–14388; d) A. Martins, M. Lautens, *Org. Lett.* **2008**, *10*, 4351–4353; e) Y. Murai, L. Wang, K. Masuda, Y. Sakihama, Y. Hashidoko, Y. Hatanaka, M. Hashimoto, *Eur. J. Org. Chem.* **2013**, *2013*, 5111–5116; f) D. Munz, M. Webster-Gardiner, R. Fu, T. Strassner, W. A. Goddard, III, T. B. Gunnoe, *ACS Catal.* **2015**, *5*, 769–775; g) O. Fischer, A. Hubert, M. R. Heinrich, *J. Org. Chem.* **2020**, *85*, 11856–11866.

[13] a) M. Zhan, R. Xu, Y. Tian, H. Jiang, L. Zhao, Y. Xie, Y. Chen, *Eur. J. Org. Chem.* **2015**, *2015*, 3370–3373; b) V. Salamanca, A. C. Albéniz, *Eur. J. Org. Chem.* **2020**, *2020*, 3206–3212.

[14] a) W. Li, J. Rabeah, F. Bourriquen, D. Yang, C. Kreyenschulte, N. Rockstroh, H. Lund, S. Bartling, A.-E. Surkus, K. Junge, A. Brückner, A. Lei, M. Beller, *Nat. Chem.* **2022**, *14*, 334–341; b) J. Magano, J. R. Dunetz, *Chem. Rev.* **2011**, *111*, 2177–2250.

[15] a) D. Hesk, *J. Labelled Compd. Radiopharm.* **2020**, *63*, 247–265; b) J. Dey, M. van Gemmeren, *Synlett* **2024**, *35*, 2191–2200; c) M. Farizyan, A. Mondal, S. Mal, F. Deufel, M. van Gemmeren, *J. Am. Chem. Soc.* **2021**, *143*, 16370–16376; d) W. J. Kerr, G. J. Knox, L. C. Paterson, *J. Labelled Compd. Radiopharm.* **2020**, *63*, 281–295; e) S. Bag, M. Petzold, A. Sur, S. Bhowmick, D. B. Werz, D. Maiti, *Chem. Eur. J.* **2019**, *25*, 9433–9437; f) V. Müller, R. Weck, V. Derdau, L. Ackermann, *ChemCatChem* **2020**, *12*, 100–104; g) R. Pony Yu, D. Hesk, N. Rivera, I. Pelczer, P. J. Chirik, *Nature* **2016**, *529*, 195–199.

[16] a) R. Zhou, L. Ma, X. Yang, J. Cao, *Org. Chem. Front.* **2021**, *8*, 426–444; b) A. Suzuki, Y. Kamei, M. Yamashita, Y. Seino, Y. Yamaguchi, T. Yoshino, M. Kojima, S. Matsunaga, *Angew. Chem. Int. Ed.* **2023**, *62*, e202214433; c) Y. Y. Loh, K. Nagao, A. J. Hoover, D. Hesk, N. R. Rivera, S. L. Colletti, I. W. Davies, D. W. C. MacMillan, *Science* **2017**, *358*, 1182–1187; d) F. Legros, P. Fernandez-Rodriguez, A. Mishra, R. Weck, A. Bauer, M. Sandvoss, S. Ruf, M. Méndez, H. Mora-Radó, N. Rackelmann, C. Pöverlein, V. Derdau, *Chem. Eur. J.* **2020**, *26*, 12738–12742; e) K. Murugesan, K. Donabauer, R. Narobe, V. Derdau, A. Bauer, B. König, *ACS Catal.* **2022**, *12*, 3974–3984.

[17] a) S. Kolb, D. B. Werz, *Chem. Eur. J.* **2023**, *29*, e202300849; b) S. Kolb, D. B. Werz, *Angew. Chem. Int. Ed.* **2024**, e202316037; c) Z. Zhao, R. Zhang, Y. Liu, Z. Zhu, Q. Wang, Y. Qiu, *Nat. Commun.* **2024**, *15*, 3832; d) K. Yang, T. Feng, Y. Qiu, *Angew. Chem. Int. Ed.* **2023**, *62*, e202312803; e) L. Shi, M. Liu, L. Zheng, Q. Gao, M. Wang, X. Wang, J. Xiang, *Org. Lett.* **2024**, *26*, 4318–4322.

[18] a) J. L. Röckl, D. Pollok, R. Franke, S. R. Waldvogel, *Acc. Chem. Res.* **2020**, *53*, 45–61; b) J. L. Röckl, M. Dörr, S. R. Waldvogel, *ChemElectroChem* **2020**, *7*, 3686–3694; c) L. Schulz, S. R. Waldvogel, *Synlett* **2019**, *30*, 275–286; d) S. R. Waldvogel, S. Lips, M. Selt, B. Riehl, C. J. Kampf, *Chem. Rev.* **2018**, *118*, 6706–6765.

[19] a) I. Colomer, A. E. R. Chamberlain, M. B. Haughey, T. J. Donohoe, *Nat. Chem. Rev.* **2017**, *1*, 0088; b) H. F. Motiwala, A. M. Armaly, J. G. Cacioppo, T. C. Coombs, K. R. K. Koehn, V. M. Norwood, J. Aubé, *Chem. Rev.* **2022**, *122*, 12544–12747; c) A. M. Arnold, P. Dullinger, A. Biswas, C. Jandl, D. Horinek, T. Gulder, *Nat. Commun.* **2023**, *14*, 813; d) A. M. Arnold, A. Poethig, M. Drees, T. Gulder, *J. Am. Chem. Soc.* **2018**, *140*, 4344–4353; e) J. Binder, A. Biswas, T. Gulder, *Chem. Sci.* **2023**, *14*, 3907–3912; f) O. Hollóczki, A. Berkessel, J. Mars, M. Mezger, A. Wiebe, S. R. Waldvogel, B. Kirchner, *ACS Catal.* **2017**, *7*, 1846–1852; g) A. Berkessel, J. A. Adrio, D. Hüttenhain, J. M. Neudörfl, *J. Am. Chem. Soc.* **2006**, *128*, 8421–8426; h) A. Berkessel, J. A. Adrio, *J. Am. Chem. Soc.* **2006**, *128*, 13412–13420; i) N. Luo, M. Turberg, M. Leutzsch, B. Mitschke, S. Brunen, V. N. Wakchaure, N. Nöthling, M. Schelwies, R. Pelzer, B. List, *Nature* **2024**, *632*, 795–801; j) M. Piejko, J. Moran, D. Lebœuf, *ACS Org. Inorg. Au* **2024**, *4*, 287–300.

[20] T. Zhang, T. Doert, H. Wang, S. Zhang, M. Ruck, *Angew. Chem. Int. Ed.* **2021**, *60*, 22148–22165.

[21] a) R. Wagner, M. Korth, B. Streipert, J. Kasnatscheew, D. R. Gallus, S. Brox, M. Amereller, I. Cekic-Laskovic, M. Winter, *ACS Appl. Mater. Interfaces* **2016**, *8*, 30871–30878; b) S. Solchenbach, M. Metzger, M. Egawa, H. Beyer, H. A. Gasteiger, *J. Electrochem. Soc.* **2018**, *165*, A3022.

[22] a) A. E. Gebala, M. M. Jones, *J. Inorg. Nucl. Chem.* **1969**, *31*, 771–776; b) E. W. C. Spotte-Smith, T. B. Petrocelli, H. D. Patel, S. M. Blau, K. A. Persson, *ACS Energy Lett.* **2023**, *8*, 347–355.

[23] M. G. Freire, C. M. S. S. Neves, I. M. Marrucho, J. A. P. Coutinho, A. M. Fernandes, *J. Phys. Chem. A* **2010**, *114*, 3744–3749.

[24] Y. A. Abdo, G. S. Tschumper, *J. Phys. Chem. A* **2020**, *124*, 8744–8752.

[25] a) F. Weigend, R. Ahlrichs, *Phys. Chem. Chem. Phys.* **2005**, *7*, 3297–3305; b) Y.-S. Lin, G.-D. Li, S.-P. Mao, J.-D. Chai, *J. Chem. Theory Comput.* **2013**, *9*, 263–272.

[26] V. Barone, M. Cossi, *J. Phys. Chem. A* **1998**, *102*, 1995–2001.

[27] G. Marchelli, J. Ingenmey, O. Hollóczki, A. Chaumont, B. Kirchner, *ChemPhysChem* **2022**, *23*, e202100620.

[28] a) N. Heine, K. R. Asmis, *Int. Rev. Phys. Chem.* **2015**, *34*, 1–34; b) S. Schmahl, F. Horn, J. Jin, H. Westphal, D. Belder, K. R. Asmis, *ChemPhysChem* **2024**, *25*, e202300975.

[29] M. Brümmer, C. Kaposta, G. Santambrogio, K. R. Asmis, *J. Chem. Phys.* **2003**, *119*, 12700–12703.

[30] M. Mayer, K. R. Asmis, *J. Phys. Chem. A* **2021**, *125*, 2801–2815.

[31] N. Heine, K. R. Asmis, *Int. Rev. Phys. Chem.* **2016**, *35*, 507–507.

[32] a) M. J. Frisch, G. W. Trucks, H. B. Schlegel, G. E. Scuseria, M. A. Robb, J. R. Cheeseman, G. Scalmani, V. Barone, G. A. Petersson, H. Nakatsuji, X. Li, M. Caricato, A. V. Marenich, J. Bloino, B. G. Janesko, R. Gomperts, B. Mennucci, H. P. Hratchian, J. V. Ortiz, A. F. Izmaylov, J. L. Sonnenberg, Williams, F. Ding, F. Lipparini, F. Egidi, J. Goings, B. Peng, A. Petrone, T. Henderson, D. Ranasinghe, V. G. Zakrzewski, J. Gao, N. Rega, G. Zheng, W. Liang, M. Hada, M. Ehara, K. Toyota, R. Fukuda, J. Hasegawa, M. Ishida, T. Nakajima, Y. Honda, O. Kitao, H. Nakai, T. Vreven, K. Throssell, J. A. Montgomery Jr., J. E. Peralta, F. Ogliaro, M. J. Bearpark, J. J. Heyd, E. N. Brothers, K. N. Kudin, V. N. Staroverov, T. A. Keith, R. Kobayashi, J. Normand, K. Raghavachari, A. P. Rendell, J. C. Burant, S. S. Iyengar, J. Tomasi, M. Cossi, J. M. Millam, M. Klene, C. Adamo, R. Cammi, J. W. Ochterski, R. L. Martin, K. Morokuma, O. Farkas, J. B. Foresman, D. J. Fox, *Gaussian 16 Rev. C.01*, **2016**, ; b) D. J. Wales, J. P. K. Doye, *J. Phys. Chem. A* **1997**, *101*, 5111–5116; c) M. J. Lecours, W. C. T. Chow, W. S. Hopkins, *J. Phys. Chem. A* **2014**, *118*, 4278–4287; d) C. Zhou, C. Ieritano, W. S. Hopkins, *Front. Chem.* **2019**, *7*.

[33] S. Grimme, S. Ehrlich, L. Goerigk, *J. Comput. Chem.* **2011**, *32*, 1456–1465.

[34] R. A. Kendall, T. H. Dunning, Jr., R. J. Harrison, *J. Chem. Phys.* **1992**, *96*, 6796–6806.

[35] https://cccbdb.nist.gov/vibscalejust.asp.

[36] a) I. E. Gordon, L. S. Rothman, R. J. Hargreaves, R. Hashemi, E. V. Karlovets, F. M. Skinner, E. K. Conway, C. Hill, R. V. Kochanov, Y. Tan, P. Wcisło, A. A. Finenko, K. Nelson, P. F. Bernath, M. Birk, V. Boudon, A. Campargue, K. V. Chance, A. Coustenis, B. J. Drouin, J. M. Flaud, R. R. Gamache, J. T. Hodges, D. Jacquemart, E. J. Mlawer, A. V. Nikitin, V. I. Perevalov, M. Rotger, J. Tennyson, G. C. Toon, H. Tran, V. G. Tyuterev, E. M. Adkins, A. Baker, A. Barbe, E. Canè, A. G. Császár, A. Dudaryonok, O. Egorov, A. J. Fleisher, H. Fleurbaey, A. Foltynowicz, T. Furtenbacher, J. J. Harrison, J. M. Hartmann, V. M. Horneman, X. Huang, T. Karman, J. Karns, S. Kassi, I. Kleiner, V. Kofman, F. Kwabia–Tchana, N. N. Lavrentieva, T. J. Lee, D. A. Long, A. A. Lukashevskaya, O. M. Lyulin, V. Y. Makhnev, W. Matt, S. T. Massie, M. Melosso, S. N. Mikhailenko, D. Mondelain, H. S. P. Müller, O. V. Naumenko, A. Perrin, O. L. Polyansky, E. Raddaoui, P. L. Raston, Z. D. Reed, M. Rey, C. Richard, R. Tóbiás, I.

Sadiek, D. W. Schwenke, E. Starikova, K. Sung, F. Tamassia, S. A. Tashkun, J. Vander Auwera, I. A. Vasilenko, A. A. Vigasin, G. L. Villanueva, B. Vispoel, G. Wagner, A. Yachmenev, S. N. Yurchenko, *J. Quant. Spectrosc. Radiat. Transfer* **2022**, *277*, 107949; b) P. E. Fraley, K. Narahari Rao, *J. Mol. Spectry.* **1969**, *29*, 348–364; c) J. R. Roscioli, E. G. Diken, M. A. Johnson, S. Horvath, A. B. McCoy, *J. Phys. Chem. A* **2006**, *110*, 4943–4952.

[37] A. J. Barnes, J. Murto, *J. Chem. Soc. Faraday Trans. 2* **1972**, *68*, 1642–1651.

[38] F. Neese, F. Wennmohs, U. Becker, C. Riplinger, *J. Chem. Phys.* **2020**, *152*, 224108.

[39] F. Neese, F. Wennmohs, A. Hansen, U. Becker, *Chem. Phys.* **2009**, *356*, 98–109.

[40] P. Pracht, F. Bohle, S. Grimme, *Phys. Chem. Chem. Phys.* **2020**, *22*, 7169–7192.

[41] a) V. Ásgeirsson, B. O. Birgisson, R. Bjornsson, U. Becker, F. Neese, C. Riplinger, H. Jónsson, *J. Chem. Theory Comput.* **2021**, *17*, 4929–4945; b) G. Henkelman, B. P. Uberuaga, H. Jónsson, *J. Chem. Phys.* **2000**, *113*, 9901–9904.

Manuscript received: September 17, 2024
Accepted manuscript online: November 20, 2024
Version of record online: December 4, 2024